EPJ A direct
electronic only

Study of the N = 28 shell closure in the Ar isotopic chain

A SPIRAL experiment for nuclear astrophysics

L. Gaudefroy[1,a], O. Sorlin[2], D. Beaumel[1], Y. Blumenfeld[1], Z. Dombrádi[3], S. Fortier[1], S. Franchoo[1], M. Gélin[2], J. Gibelin[1], S. Grévy[2], F. Hammache[1], F. Ibrahim[1], K. Kemper[4], K.L. Kratz[5], S.M. Lukyanov[6], C. Monrozeau[1], L. Nalpas[7], F. Nowacki[8], A.N. Ostrowski[5], Yu.-E. Penionzhkevich[6], E. Pollacco[7], P. Roussel-Chomaz[2], E. Rich[1], J.A. Scarpaci[1], M.G. St. Laurent[2], T. Rauscher[9], D. Sohler[3], M. Stanoiu[1], E. Tryggestad[1], and D. Verney[1]

1 IPN, IN2P3-CNRS, F-91406 Orsay Cedex, France
2 GANIL, BP 55027, F-14076 Caen Cedex 5, France
3 Institute of Nuclear Research, H-4001 Debrecen, Pf. 51, Hungary
4 Department of Physics, Florida State University, Tallahassee, FL 32306, USA
5 Institut für Kernchemie, Universität Mainz, D-55128 Mainz, Germany
6 FLNR/JINR, 141980 Dubna, Moscow Region, Russia
7 CEA-Saclay, DAPNIA-SPhN, F-91191 Gif-sur-Yvette Cedex, France
8 IReS, Univiversité Louis Pasteur, BP 28, F-67037 Strasbourg Cedex, France
9 Departement für Physik und Astronomie, Universität Basel, Switzerland

Abstract. The structure of the neutron-rich nucleus ^{47}Ar has been investigated through the d(^{46}Ar,^{47}Ar)p transfer reaction. The radioactive beam of ^{46}Ar at $10\,A \cdot \mathrm{MeV}$ was provided by the SPIRAL facility at GANIL. The protons corresponding to a neutron pick-up on bound or unbound states mechanism in ^{47}Ar nuclei were detected at backward angles by the position-sensitive Si array-detector MUST. The transfer-like ejectiles were detected in the SPEG spectrometer. Level scheme, spin assignments and spectroscopic factors have been deduced for ^{47}Ar and compared to shell model predictions. They suggest a slight erosion of the $N = 28$ shell gap from the weakening of the spin-orbit interaction arising from the f and p orbitals. These spectroscopic information are subsequently used to infer (n,γ) reaction rates in the Ar isotopic chain to understand the origin of the ^{48}Ca/^{46}Ca abnormal isotopic ratio observed in certain inclusions of meteorites.

PACS. 21.10.Hw Spin, parity, and isobaric spin – 21.10.Jx Spectroscopic factors – 25.60.Je Transfer reactions – 26.30.+k Nucleosynthesis in novae, supernovae and other explosive environments

1 Introduction

The role of the spin-orbit interaction is essential to create the magic numbers as $N = 28$, revealed for instance in the doubly magic nucleus ^{48}Ca. This interaction lowers the $f_{7/2}$ neutron orbit just into the middle of the gap between the sd and fp oscillator shells, resulting in a neutron magic number at $N = 28$. The ordering of the neutron orbitals around $N = 28$ ($f_{7/2}$, $p_{3/2}$, $p_{1/2}$ and $f_{5/2}$) exhibits 2 pairs of spin-orbit partners originating from the f and p states. A differential change in the size of these two pairs of orbitals could enhance or reduce the $N = 28$ gap. A strong reduction of the f spin-orbit splitting, as compared to the p one, would erode the $N = 28$ gap. This would create particle-hole (ph) excitations between orbitals of the same oscillator shell $f_{7/2}$ and $p_{3/2}$ which are strongly

connected by quadrupole interactions. Thus, even a small amount of excitations across $N = 28$ may lead to permanent quadrupole deformation. Therefore, the emergence of deformed nuclei with $N = 28$ is intimately related to the strength of the spin-orbit interaction.

Recent experimental data suggest an erosion of the $N = 28$ shell in very neutron-rich nuclei. According to β-decay [1] and Coulomb-excitation [2] experiments, quadru- pole ground-state deformation develops at $Z = 16$ four protons below the doubly magic ^{48}Ca. Study of the neutron-rich $^{40-44}$S using the in-beam γ-spectroscopy technique [3] suggests deformed ground states for ^{40,42}S and a mixed deformed configuration for ^{44}S in accordance with both the mean-field [4,5,6,7,8] and the recent large-scale shell model calculations [9]. A 0_2^+ level (of mainly 2p2h origin) was tentatively assigned at an energy of 2.7 MeV in ^{46}Ar [10], as compared to 4.28 MeV in ^{48}Ca. The recent finding of a 0_2^+ at 1.365 keV in ^{44}S shows that

a e-mail: gaudefroy@ganil.fr

the decrease of the 0_2^+ level has continued with the removal of protons in the sd shell. The large $\rho^2(E0 : 0_2^+ \rightarrow 0_1^+)$ points towards the existence of two strongly interacting states with very different shapes in ^{44}S. This witnesses that the $N = 28$ gap has been overcome by ph excitations to generate permanent quadrupole deformation.
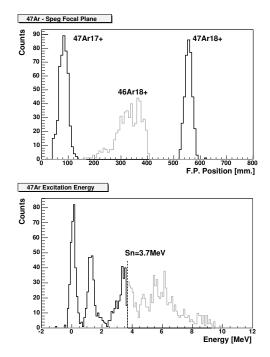
To understand the erosion of the $N = 28$ shell gap south to ^{48}Ca, and its probable link to a reduced spin-orbit splitting, it is essential to see the evolution of the $f_{7/2}$, $p_{3/2}$, $p_{1/2}$ and $f_{5/2}$ orbitals in the ^{46}Ar nucleus. The tensor monopole interaction [11] could be responsible for this reduction. It acts in the present case between the protons in the sd shell (mainly in the $d_{3/2}$ orbital) and the neutrons in the two $f_{7/2}$-$f_{5/2}$ and $p_{3/2}$- $p_{1/2}$ spin-orbit partners. As protons are removed from the $d_{3/2}$ orbital, the spin-orbit splittings are weakened. To see if such an effect is observed in the $N = 28$ region we should compare the neutron single-particle energies in the ^{49}Ca and ^{47}Ar isotones. In ^{49}Ca the size of the spin-orbit splitting between the p orbits is of about $2\,\mathrm{MeV}$, and the main component of the $f_{5/2}$ strength lies at $3.9\,\mathrm{MeV}$ excitation energy (referenced to the $p_{3/2}$ ground state (g.s.)). The present goal of the d(^{46}Ar,^{47}Ar)p transfer reaction is to obtain similar information in ^{47}Ar. To achieve this goal, we have used the newly operating SPIRAL facility to produce a radioactive beam of ^{46}Ar.

The study of the $N = 28$ shell closure is expected to shed some light on the hitherto mysterious anomalies observed in certain meteorites, as the large ^{48}Ca/^{46}Ca ratio. The present study aims to deduce radiative neutron-capture rates in the Ar isotopic chain from the spectroscopic information obtained through the (d, p) transfer reaction. Astrophysical consequences are subsequently discussed.

2 Experimental methods

The transfer reaction d(^{46}Ar,^{47}Ar)p has been performed at GANIL with a radioactive beam of ^{46}Ar produced by the SPIRAL facility. This beam has been produced through the projectile fragmentation of a $66\,A \cdot \mathrm{MeV}$ ^{48}Ca primary beam of about $200\,\mathrm{pnA}$ intensity in a thick carbon target located at the underground production cave of SPIRAL. The isotopes of interest were produced into the target which was heated at $2000\,\mathrm{K}$ in order to favor their extraction. They were subsequently ionized by an ECR source to the charge 9^+ and accelerated by the cyclotron CIME up to the energy of $10\,A \cdot \mathrm{MeV}$. The beam intensity of ^{46}Ar was $2 \cdot 10^4\,\mathrm{s}^{-1}$, without isobaric contamination. In addition to this, a stable beam of ^{40}Ar has been produced by the same devices at similar energy in order to validate our analysis of the pick-up (d, p) reaction with a known case studied in direct kinematics [12]. The total number of ^{40}Ar and ^{46}Ar nuclei which crossed the target was $2 \cdot 10^9$ and $4 \cdot 10^9$, respectively.

Neutron pick-up reactions (d, p) were induced by a $380\,\mu\mathrm{g} \cdot \mathrm{cm}^{-2}$ thick CD$_2$ target. The tracking of the secondary beams was achieved by a position-sensitive gas-filled detector CATS [13] located $11\,\mathrm{cm}$ downstream the

Fig. 1. Top: Position of the nuclei transmitted in the focal plane of SPEG for the ^{46}Ar (d, p) ^{47}Ar reaction. The grey line indicates transfer above the neutron separation energy S_n. The bottom part shows the corresponding energy spectrum.

target. We have reconstructed the impact points of the nuclei on the target with an accuracy of $1.0\,\mathrm{mm}$. Protons were detected at backward angles (between 110 and 170 degrees) using the 8 position-sensitive MUST telescopes [14]. By measuring the energies (from 0.3 to $6\,\mathrm{MeV}$) and angles of the protons, the two-body pick-up reaction can be characterized. The beam-like transfer products were selected by the SPEG [15] spectrometer and identified at its dispersive focal plane through their position (see fig. 1 top), energy loss and time-of-flight information. In order to obtain the energy spectrum of ^{47}Ar (^{46}Ar), we have used the measured proton energy and angle in the relativistic kinematics formula.

The experimental proton angular distributions have been compared to those obtained with DWBA calculations using the DWUCK4 code [16] to deduce the ℓ value and spectroscopic factor (SF) of each identified level (fig. 2). Several optical potentials have been used to see their influence on the SF values. It was found that, depending on the potential, the SF vary within about 20% around a mean value. We have considered two different potentials for both the entrance and exit channels, and used the four combinations between them to describe the (d, p) reaction. The (d+^{46}Ar) channel was described by using the deuteron global optical potential parametrization of W.W. Daehnick et al. [17] (denoted as D1 in the following) or the adiabatical deuteron potential of G.L. Wales and R.C. Johnson [18] (D2) which takes into account the effect of the deuteron break-up. The deuteron potential is described with a combination of neutron and proton potentials (CH89 [19]) for the parametrization of the break-up.
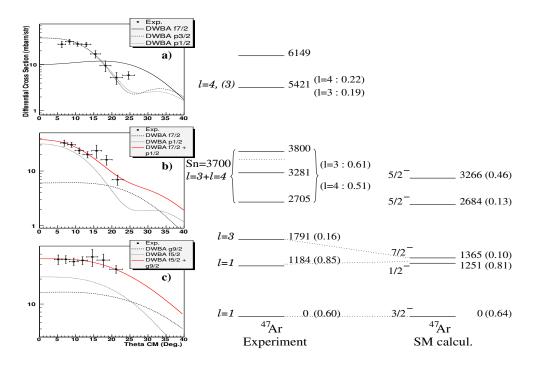
Fig. 2. Left: Angular distributions for the g.s. **a)**, $1^{st} + 2^{nd}$ excited states **b)** and the structure around 3.5 MeV (3 states) **c)** in ^{47}Ar are shown in comparison to DWBA calculations assuming $\ell=1$, 3 or 4 distributions. Right: Experimental level scheme in ^{47}Ar obtained from the present work compared to shell model calculations using the sdpf interaction [25]. Calculated and experimental spectroscopic factors are indicated in parentheses. Only calculated levels with spectroscopic factors greater than 0.1 are presented.

The exit channel (p+^{47}Ar) was described both by the potential CH89 (denoted as P1) and by the parametrization of C.M. Perey and F.G. Perey [20] (P2).

3 Experimental results

The energy spectrum of ^{47}Ar is shown in fig. 1 bottom. Prior to the present work only the mass excess (Δm) and beta-decay half-life of ^{47}Ar were known. However, the use of tabulated value $\Delta m = -25.9(1)$ MeV for ^{47}Ar [21] would shift by 600 keV the peak corresponding to the $p_{3/2}$ ground state (g.s.). Since the method to deduce the excitation spectrum has been proven to be successful already to deduce the whole excitation spectra of ^{41,45}Ar [22], we would suggest a new mass-excess value of $\Delta m = -25.3(2)$ MeV for ^{47}Ar to bring back the g.s. level to zero excitation energy as shown in fig. 1. This new mass-excess leads to a neutron separation energy (S_n) in ^{47}Ar of 3.7(2) MeV instead of 4.25(14) MeV. The full width at half maximum of the g.s. peak is 420 keV. With this energy resolution, an unfolding procedure is often required to separate several peaks which lie at nearby energies. Two Gaussian distributions centered at 1.1(2) and 1.8(2) MeV are used to reproduce the observed structure between 0.8 and 2.2 MeV. In the same manner, three Gaussians centered at 2.7(2), 3.3(2) and 3.8(2) MeV are required to reproduce the broad structure around 3 MeV. As in the case of ^{45}Ar [22], well-defined structures are still visible in ^{47}Ar above the neutron separation energy value S_n. This indi-

Table 1. Spectroscopic factors obtained in the data analysis of the ^{46}Ar(d, p)^{47}Ar reaction with combinations of the four optical potentials D1, D2, P1 and P2 described in the text.

E^* (keV)	D1P1	D1P2	D2P1	D2P2
0 ($p_{3/2}$)	0.60	0.53	0.65	0.57
1184 ($p_{1/2}$)	0.93	0.81	0.84	0.77
1791 ($f_{7/2}$)	0.17	0.13	0.20	0.18
2705-3800 ($\ell = 3,4$)	$\ell = 3 : 0.57$ $\ell = 4 : 0.51$	0.57 0.44	0.66 0.58	0.66 0.53
5421 ($\ell = 3,4$)	$\ell = 3 : 0.17$ $\ell = 4 : 0.21$	0.17 0.20	0.19 0.23	0.20 0.22

cates that at this energy, the level scheme cannot be considered as a continuum of states. We note however that the spectrum cannot be exploited above 6 MeV in ^{47}Ar because it is obtained with protons whose energies become too low to be detected at the most backward angles of the MUST detector.

Angular distributions have been deduced for all states but the one at 6.1(2) MeV. The spectroscopic factors listed in table 1 have been extracted using the procedure described in section 2. The g.s. exhibits an angular distribution which is typical of an $\ell = 1$ state. This is in agreement with the $p_{3/2}$ assignment obtained with the Shell Model (SM) calculations using the ANTOINE code [23,24] with the *sdpf* interaction [25] (see fig. 2). The spectroscopic

factors of the $p_{3/2}$ is 0.6 in ^{47}Ar as compared to 0.84 in the isotone ^{49}Ca. Two components of orbital momenta $\ell = 1$ and $\ell = 3$ have to been used to fit the states at 1.1(2) MeV and 1.8(2) MeV. We tentatively assign the configurations $p_{1/2}$ and $f_{7/2}$ to the states at 1.1(2) MeV and 1.8(2) MeV, respectively. The spectroscopic factor of the $p_{1/2}$ state is close to unity, indicating its quasi-pure single neutron configuration added to the ^{46}Ar core. The intruder state $7/2^-$ built on a $(\nu p_{3/2})^2 (\nu f_{7/2})^{-1}$ configuration has a spectroscopic factor of 0.16 in ^{47}Ar. The experimental energies and spectroscopic factors of the g.s. and first excited states compare very well with SM calculations. The SF value of the intruder configuration also agrees very well, but the level lies about 400 keV above the calculated value. This indicates that SM calculations either slightly underestimate the size of the $N = 28$ gap or overestimate pairing/correlation energies gained by promoting a neutron in the $p_{3/2}$ orbital in ^{47}Ar. The present result will help for better understanding the onset of collectivity in the $Z = 16$ nuclei through intruder excitations. It is also interesting to compare the spin-orbit splitting between the $p_{1/2}$ and $p_{3/2}$ states which is reduced from about 2 MeV in ^{49}Ca to 1.2 MeV in ^{47}Ar, as two protons are removed from the quasi-degenerated proton $d_{3/2}$ and $s_{1/2}$ orbitals. The origin of this decrease of spin-orbit splitting with the removal of $d_{3/2}$ protons could be ascribed to the tensor monopole force [11] which acts in opposite sign between the two orbitals $p_{1/2}$ and $p_{3/2}$.

The fit of the experimental angular distribution located around 3 MeV excitation energy requires the presence of at least three states, and an admixture of $\ell = 3$ and/or $\ell = 4$ components as shown in table 1. This is in nice agreement with the SM calculations. Another solution of the fit leads to a much higher $\ell = 4$ SF of 0.76. However this value is very unlikely as the SF of the $g_{9/2}$ orbital is weaker than 0.2 in ^{49}Ca and never exceeds 0.6 at that excitation energy in the $N = 29$ isotones. From the present assumption, it is found that the components of the $f_{5/2}$ orbital are lowered by about 500 keV between ^{49}Ca and ^{47}Ar. This could be an effect of the reduction of the spin-orbit splitting between the $f_{7/2}$ and $f_{5/2}$ orbitals, which is evidenced through the lowering of the $f_{5/2}$ orbital with respect to the $p_{3/2}$ g.s.

We have used the same interaction, $sdpf$, to calculate the level scheme of ^{49}Ar (fig. 3), which is currently not reachable via (d, p) reaction as the intensity of ^{48}Ar beam is too weak. Given the good agreement between calculated and experimental levels in ^{45,47}Ar (see ref. [22] for ^{45}Ar), we expect to obtain reliable predictions for the case of ^{49}Ar whose astrophysical interest will be emphasized in the next section. This nucleus exhibits two low-energy $p_{3/2}$ and $p_{1/2}$ states with SF of 0.23 and 0.77, respectively. In ^{48}Ar$_{30}$ the $p_{3/2}$ is in principle half-filled. Therefore a SF of 0.23 carries about 50% of the $p_{3/2}$ total strength. The first excited state carries almost all the $p_{1/2}$ strength. It is shifted down by about 1 MeV as compared to the ^{47}Ar because of the pairing energy gain of the 2 holes in the $p_{3/2}$ orbital when promoting a neutron in the $p_{1/2}$ shell.
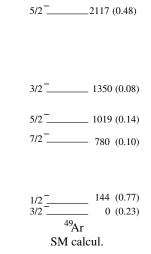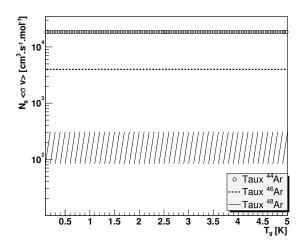

Fig. 3. Calculated level scheme and spectroscopic factors (in parenthesis) of ^{49}Ar.

4 Determination of (n, γ) rates from (d, p) reaction

The experimental results obtained on ^{45,47}Ar nuclei from (d, p) reactions are used in the following to determine the neutron capture rates (n, γ) on ^{44,46}Ar. Similar procedure is applied to determine ^{48}Ar(n, γ) capture rate using the calculated structure of ^{49}Ar. This will bring a wealth of data to be used for a possible explanation of the abnormally high abundance ratio ^{48}Ca/^{46}Ca observed in certain refractory inclusions of meteorites. We have applied a procedure similar to that described in ref. [26] for the case of ^{48}Ca to calculate the neutron capture cross section in the Ar isotopic chain. It was pointed out in ^{48}Ca that 95% of the cross section is of Direct Capture (DC) origin, which was ascribed to the intrinsic structure of the ^{49}Ca g.s. which exhibits a low angular momentum and a large spectroscopic factor. The contribution of resonant capture to unbound states was negligible since the level density at the S_n value is low. Predictions in the Ar isotopic chain around $N = 28$ depend strongly on the nuclear structure of ^{46}Ar nucleus. In particular, the neutron-capture rates depend on the SF of the low-energy p states, the S_n value and the level density above the latter. These three points are examined in the following.

Taking into account the spin-conservation rules in the DC reaction, the neutron is mainly captured into $\ell = 1$ bound states through the $E1$ operator without centrifugal barrier as the transferred angular momentum is $\ell_n = 0$ (s-wave capture). The ratio between s-wave (final state with $\ell = 1$) and d-wave (final state with $\ell = 3$) direct neutron-capture rate is approximately 10^4 in the present nuclei [27]. Therefore the s-wave DC to the g.s. and first excited states that have both large spectroscopic factors and $\ell = 1$ values dominates over all other contributions. Moreover, in an s-wave capture, the velocity dependence of the cross section is known to be $1/v$, and the Maxwell-average neutron capture rate (MACS $= Na\langle\sigma v\rangle$, with Na

Fig. 4. From top to bottom curves: neutron capture rates on ^{44,46,48}Ar deduced from our results (for ^{44,46}Ar) and from SM calculations (for ^{48}Ar). The dashed region witnesses the large uncertainty on the S_n value of ^{49}Ar.

the Avogadro number) is not expected to show energy dependence.

The neutron separation energy S_n in the final nuclei is also a key ingredient to determine the direct neutron-capture rate. It defines the Q-value of the (n, γ) reaction to the bound states in the ^{45,47,49}Ar nuclei. Owing to the known mass-excesses of ^{44,45,46}Ar and the newly determined one of ^{47}Ar, we can determine the reaction Q-values for the ^{44,46}Ar neutron captures with sufficient precision. In the case of ^{49}Ar, only extrapolated value exists [21]. The large uncertainty of about $800 \, \mathrm{keV}$ on the Q-value $(2.5(8) \, \mathrm{MeV}$ for a capture to the g.s.) implies a large uncertainty in the calculation of the neutron-capture rate on ^{48}Ar, as shown in fig. 4.

Well-defined energy peaks are still present above the neutron emission threshold in both ^{45}Ar and ^{47}Ar nuclei. This means that the statistical treatment of neutron captures using the Hauser-Feshbach formalism is no longer valid for these light nuclei, close to magic numbers. Instead, individual resonances should be considered. As the centrifugal barrier will strongly hinder neutron-captures on orbitals of high angular momenta, we have to search for resonances with low-ℓ values in the vicinity of the neutron separation energy. As mentioned above, no state with $\ell \leq 1$ has been found, making the resonant capture a negligible process for these nuclei.

The direct neutron capture rates on ^{44,46}Ar have been calculated using the procedure described in ref. [26] and the experimental spectroscopic information presented here and in ref. [22]. As the DC process mainly occurs at the surface of the nucleus, the choice of an appropriate nuclear density distribution is important. These have been obtained from mean-field calculations using HFB formalism in a spherical geometry [28]. These distributions reproduce remarkably well the measured root mean square radii of ^{44,46}Ar [29]. The neutron capture rate on ^{48}Ar was deduced from the calculated structure of ^{49}Ar, presented in the previous section. The calculated MACS are shown

in fig. 4. A MACS ratio of about 5 occurs between $A = 44$ and $A = 46$, and a more pronounced one (10 to 50 depending on the S_n value in ^{49}Ar) between $A = 46$ and $A = 48$. Mass measurements of the neutron-rich ^{48,49}Ar isotopes are of great interest to infer the ^{48}Ar(n, γ) rate with better accuracy. From our results summarized in fig. 4, it arises that nuclear structure (*i.e.* the presence of low angular momenta states — $\ell = 1$ — with closed to one SF and high binding energies) speed-up the neutron capture at $A = 46$ (as compared to $A = 48$), despite the presence of the $N = 28$ shell closure.

5 Astrophysical implications

About two decades ago, G.J. Wasserburg and his group at Caltech identified correlated isotopic anomalies for the neutron-rich ^{48}Ca, ^{50}Ti and ^{54}Cr isotopes in peculiar refractory inclusions of the Allende meteorite [30,31]. As an example, the ^{48}Ca/^{46}Ca ratio was found to be 250, a factor of 5 larger than in the Solar System. It was concluded that these highly unusual isotopic compositions witness late-stage nucleosynthesis processes which preceded the formation of the solar nebula. However, astrophysical models existing at that time encountered severe difficulties when trying to reproduce these observed anomalies, in particular those in the EK-1-4-1 inclusions. Since that time major progresses have been made in particular on mass measurements, β-decay lifetimes of unstable nuclei and neutron-capture cross sections on stable and unstable nuclei (present work). We now gather all information to see which stellar conditions could account for these observations.

A plausible astrophysical scenario to account for the overabundance of ^{48}Ca is a weak rapid neutron-capture process [32,27]. There the neutron-rich stable ^{46,48}Ca isotopes are produced during a neutron-capture and β-decay process. The main contribution to the production of these Ca isotopes is provided by the β-decay of their progenitor isobars in the Ar isotopic chain [27]. This was traced back from the fact that, in the $Z < 18$ chains, the measured β-decay lifetimes of ^{44}S and ^{45}Cl are shorter than the neutron-capture rates at the $N = 28$ shell closure. Consequently, the matter flow in the S and Cl chains is depleted by β-decay to the upper Z isotopes before reaching masses $A = 46$ or 48. It was noted earlier that this feature arises from the erosion of the $N = 28$ shell gap in the S and Cl isotopic chains [1]. Thus the main progenitors of ^{46,48}Ca are produced either directly in the Ar chain or from the β-decay of $Z < 18$ nuclei which subsequently could capture neutrons in the Ar chain. Therefore the determination of neutron-capture rates in the Ar isotopes is important. Competition between the neutron capture and β-decay reactions is reflected by the reaction mean times. The mean neutron capture time t_n can be expressed as $t_n = 1/(d_n \langle \sigma v \rangle)$. Knowing the β-decay half lives and neutron capture rates in the nuclei of interest, we can deduce an approximative value of the neutron density, d_n, which could account for the large observed isotopic ratio ^{48}Ca/^{46}Ca $= 250$ in the weak r-process

Table 2. Neutron capture and β decay mean times for $A = 44$, 46 and 48 in the argon chain. The neutron capture mean times are deduced from the present work. The mean rate value of ^{49}Ar has been taken to deduce its neutron capture mean time.

Isotope	$Na\langle\sigma v\rangle$	t_n	$T_{1/2}^{\beta}$
^{44}Ar	$6.19\ 10^6$	$2.8\ 10^{-5}$ s	11.9 min
^{46}Ar	$4.04\ 10^3$	45 ms	7.8 s
^{48}Ar	$2.03\ 10^2$	1 s	0.45 s

temperature range ($T_9 = 0.1$ to $\simeq 5$). Such a neutron density would give rise to a neutron capture mean time, $t_n^{46\text{Ar}}$, on ^{46}Ar which favors the capture reaction in comparison to the β-decay one. This can be expressed by the relation $1 - \exp(\frac{-\ln 2 \cdot t_n^{46\text{Ar}}}{7.8}) = 1/250$ which leads to a $t_n^{46\text{Ar}}$ value of about 45 ms implying a neutron density of about $3 \cdot 10^{21}$ cm^{-3}. Table 2 presents the neutron capture mean times corresponding to that neutron density, as well as the β-decay half lives.

At $A = 48$, calculated t_n becomes longer than $T_{1/2}^{\beta}$. Consequently the neutron capture is halted in the Ar chain at $A = 48$, accumulating substantial amount of ^{48}Ca. Conversely, few depletion occurs through β-decay at $A = 46$ as the lifetime of ^{46}Ar is longer than neutron capture time. These two features can account for explaining the observed high ^{48}Ca/^{46}Ca ratio. More realistic nucleosynthesis network calculations are in progress in order to confirm or otherwise the naive picture drawn.

6 Conclusions

Spectroscopic information has been obtained in ^{47}Ar$_{29}$ using the d(^{46}Ar,^{47}Ar)p transfer reaction at GANIL/SPIRAL. We have used the position-sensitive MUST detector for the protons and the SPEG spectrometer to select and identify the transfer-like nuclei ^{47}Ar. Energies and angular distributions of hitherto unknown levels in ^{47}Ar have been determined for the first time. A new value of the mass-excess of ^{47}Ar, $\Delta m = -25.3(2)$ MeV, is proposed. The two components of the spin-orbit splitting $p_{3/2}$ and $p_{1/2}$ have been identified at low excitation energies in ^{47}Ar. The approximate location of the $f_{5/2}$ strength has been determined too. These data point to a weakening of the p and f spin-orbit splittings, the latter being responsible for the reduction of the $N = 28$ shell gap. The intruder configuration $2p1h$ across the $N = 28$ gap has been observed at 1.8(2) MeV. Its energy will constrain the size of the $N = 28$ gap in ^{47}Ar and the amount of correlations. Comparison between experimental results and shell model calculations shows a very good agreement, except for the location of the intruder state whose calculated energy is 400 keV lower. Combining the present information and the one

obtained on ^{45}Ar$_{27}$ [22], we deduce that the magicity at the $N = 28$ shell closure is preserved at ^{46}Ar. The stellar neutron capture rates ^{44,46}Ar(n,γ)^{45,47}Ar have been deduced using our data obtained from the (d, p) reaction. A nearby extrapolation led to the estimation of ^{48}Ar(n,γ)^{49}Ar rate. It is shown that nuclear structure does matter for a correct determination of these capture rates. A fast(slow) neutron-capture rate is found for ^{46}Ar(^{48}Ar). In a weak r-process scenario, with neutron density of about $3 \cdot 10^{21}$ cm^{-3}, the matter flow in the Ar chain is slightly depleted at $A = 46$ and accumulated at $A = 48$. This would result, after β-decay of the unstable Ar isotopes to an overproduction of the stable ^{48}Ca as compared to ^{46}Ca, as is observed in certain refractory inclusions of the Allende meteorite.

References

1. S. Grévy *et al.*, Phys. Lett. B **594**, 252 (2004).
2. T. Glasmacher *et al.*, Phys. Lett. B **395**, 163 (1997).
3. D. Sohler *et al.*, Phys. Rev. C **66**, 054302 (2002).
4. T.R. Werner *et al.*, Nucl. Phys. A **597**, 327 (1996).
5. P.-G. Reinhardt *et al.*, Phys. Rev. C **60**, 014316 (1999).
6. S. Péru *et al.*, Eur. Phys. J. A **49**, 35 (2000).
7. R. Rodriguez-Guzman *et al.*, Phys. Rev. C **65**, 024304 (2002).
8. G.A. Lalazissis *et al.*, Phys. Rev. C **60**, 014310 (1999).
9. E. Caurier *et al.*, Eur. Phys. J. A **15**, 145 (2002).
10. Z. Dombrádi *et al.*, Nucl. Phys. A **727**, 195 (2003).
11. T. Otsuka *et al.*, *Proceedings of the XXXIX Zakopane School of Physics*, Acta Phys. Pol. B **36**, 1213 (2005).
12. S. Sen *et al.*, Nucl. Phys. A **250**, 45 (1975).
13. S. Ottini-Hustache *et al.*, Nucl. Instrum. Methods A **431**, 476 (1991).
14. Y. Blumenfeld *et al.*, Nucl. Instrum. Methods A **421**, 471 (1999).
15. L. Bianchi *et al.*, Nucl. Instrum. Methods A **276**, 509 (1989).
16. P.D. Kunz, computer code DWUCK4, Colorado University, unpublished.
17. W.W. Daehnick *et al.*, Phys. Rev. C **21**, 2253 (1980).
18. G.L. Wales, R.C. Johnson, Nucl. Phys. A **274**, 168 (1976).
19. R.L. Varner *et al.*, Phys. Rep. **201**, 57 (1991).
20. C.M. Perey, F.G. Perey, At. Data Nucl. Data Tables **17**, 1 (1991).
21. G. Audi *et al.*, Nucl. Phys. A **729**, 3 (2003).
22. L. Gaudefroy *et al.*, J. Phys. G, to be published.
23. E. Caurier, Shell Model code ANTOINE, IReS, Strasbourg 1989-2002.
24. E. Caurier, F. Nowacki, Acta Phys. Pol. B **30**, 705 (1999).
25. S. Nummela *et al.*, Phys. Rev. C **63**, 044316 (2001).
26. E. Kraussmann *et al.*, Phys. Rev. C **53**, 469 (1996).
27. O. Sorlin *et al.*, C.R. Phys. **4**, 541 (2003).
28. M. Girod, private communication.
29. A. Klein *et al.*, Nucl. Phys. A **607**, 1 (1996).
30. T. Lee *et al.*, Astrophys. J. **220**, L21 (1978).
31. F.R. Niederer *et al.*, Astrophys. J. **240**, L73 (1980).
32. K.L. Kratz *et al.*, Mem. Soc. Astron. Ital. **2**, 453 (2001).